Advanced Steel Construction – Vol. 18 No. 4 (2022) 783–792
DOI:10.18057/IJASC.2022.18.4.6

STUDY ON STATIC AND DYNAMIC EXPERIMENT OF SPATIAL CABLE-TRUSS STRUCTURE WITHOUT INNER RING CABLES BASED ON GRID-JUMPED LAYOUT OF STRUTS

Jian Lu, Su-Duo Xue *, Xiong-Yan Li and Qing Liu

College of Civil and Architecture Engineering, Beijing University of Technology, China
** (Corresponding author: E-mail: sdxue@bjut.edu.cn)*

ABSTRACT

Cable-truss tensile structures are one of the most imperative types of spatial structures, and a spatial cable-truss structure without inner ring cables (SCSWIRC) is a new type of cable-truss tensile structure. Although SCSWIRC has a strong anti-collapse capacity, its construction forming is difficult. Based on the concept of grid-jumped layout for struts, the experimental model with a span of 6 m is designed, and then three grid-jumped layout schemes are proposed to simplify structure system. The static and dynamic properties of experimental and finite element models are systematically studied. The results show that experimental values agree with simulation values. The errors of the static experiment are in the range of 6%~11.53% and the errors of the dynamic experiment are in the range of 5%~8%. The grid-jumped layout has negligible effects on the internal forces of cables. However, it has excellent effects on the internal forces of struts and nodal displacements at the grid-jumped layout, so the mechanical property of struts needs to be rechecked after grid-jumped layout. The mechanical property of the optimal grid-jumped layout scheme does not change compared with original scheme. The optimal grid-jumped layout scheme not only simplifies SCSWIRC, but also reduces the amount of steel. The study can promote the application of SCSWIRC in practical engineering.

ARTICLE HISTORY

Received: 22 February 2022
Revised: 19 May 2022
Accepted: 22 May 2022

KEYWORDS

Spatial cable-truss structure without inner ring cables;
Structural simplification;
Grid-jumped layout;
Static and dynamic property;
A technical paper

1. Introduction

With the development of economy and technology, more and more large-span stadiums are built in the world [1, 2]. Cable-strut tensile structure [3, 4], an essential part of large-span spatial structures, is well known in the construction industry for its light weight, beautiful appearance, fast construction speed, large-spanning ability. Meanwhile, cable-strut tensile structures include many different types of structure, and cable-truss tensile structure is one of the most competitive types in cable-strut tensile structures [5, 6]. Cable-truss tensile structures are generally composed of planar cable-truss frames according to certain layout principles, and one of its common points is that the whole structure can be divided into the same kind of planar cable-truss frames. Meanwhile, planar cable-truss frame shares common characteristics, such as light weight, high stiffness, large-spanning ability and rapid construction speed. At present, cable-truss tensile structures mainly include: spoke cable-truss structure [7, 8], spatial cable-truss structure without inner ring cables (SCSWIRC) [9, 10], and so on.

Spoke cable-truss structures have many advantages of tensile structures, so many practical projects are built in the world, like Foshan Stadium [11], Shenzhen Baoan Stadium [12], Yueqing Stadium [13], Busan Stadium in South Korea [14]. Meanwhile, there are many static and dynamic experimental studies and numerical studies on spoke cable-truss structures [11, 13]. It is found from the existing studies that although the spoke cable-truss structure has many advantages, its progressive collapse ability is weak. The inner ring cable is the crucial component of spoke cable-truss structures, and the rupture of inner ring cables will result in the whole structural failure. SCSWIRC is a new type of cable-truss tensile structure, which is proposed based on the problem of weak progressive collapse ability of spoke cable-truss structures [15, 16]. At present, SCSWIRC is still in the theoretical and experimental research stage, and there are no project cases in the world. Meanwhile, there are still many unfinished studies on SCSWIRC, including how to simplify structure system, how to solve self-stress mode, how to construct forming, and so on. It is found from further studies that although SCSWIRC has a solid progressive collapse capacity, its construction forming is too difficult. With the increase in the span of SCSWIRC, the number and length of struts will be enlarged, and serious collision and winding of struts occur during construction due to SCSWIRC formed by a series of planar cable-truss frames interwoven with each other, which cause many difficulties during construction. If there is a feasible way to reduce the number of struts, it will simplify its construction process, and structural self-weight will be reduced at the same time. Based on the problem of construction forming for SCSWIRC, a grid-jumped layout is proposed to remove the redundant struts, further simplify SCSWIRC and reduce structural self-weight. Grid-jumped layout refers to removing the struts of SCSWIRC but does not destroy the structural integrality. However, the influences of grid-jumped layout on the mechanical property of SCSWIRC are unknown for designers, so it is necessary to study the effects of grid-jumped layout on SCSWIRC through numerical analysis and experimental research.

In the paper, the experimental model with a span of 6 m is firstly built for SCSWIRC. Secondly, three grid-jumped layout schemes are proposed based on experimental model. Thirdly, the static and dynamic properties of three grid-jumped layout schemes and original scheme are compared and studied by theory and experiment. Grid-jumped layout method for large-span SCSWIRC is given. Finally, the main conclusions of the paper are given. Research contents provide a simplified method and promote the application of SCSWIRC in practical engineering.

2. Design and analysis of experimental and FEM model

2.1. Design of experimental and FEM model

In order to study the influence of grid-jumped layout on SCSWIRC, the experimental model with a span of 6 m is designed for SCSWIRC. The experimental model comprises 10 planar cable-truss frames wound and interwoven with each other. Namely, the equivalent ring fractions are 10. The outer shapes of upper and lower chord cables conform to the shape of parabola, and the equations of the parabola are shown in Eq. (1). It can be seen from Ref. [17] that the optimal rise-span ratios of upper and lower chord cables are 1/25~1/20 and 1/20~1/15, respectively. So, the rise-span ratios of upper and lower chord cables for the experimental model are selected as 1/24 and 1/16. Based on structural control parameters including Eq. (1), span, ring equivalent fractions and rise-span ratios, the coefficients of Eq. (1) are obtained, namely A1=-0.091778, B1=0.075665, A2=0.137668, B2=-0.113497. The procedure of solving nodal coordinates is compiled based on structural control parameters and Fortran Language. The finite element model (FEM) is built by the nodal coordinates, and then integral FEM is built considering ring beam and supported column, shown in Fig. 1a. The size and element number of single planar cable-truss frame are shown in Fig. 1b. The feasible pre-stress values are obtained by Ref. [18], which is shown in Table 1.

$$\begin{cases} y_1 = A_1 x_1^2 + B_1 \\ y_2 = A_2 x_2^2 + B_2 \end{cases} \tag{1}$$

Based on FEM, the integral experimental model is designed, including the main cable system structure, cable-strut joint, cable-beam joint, ring beam and supported column, shown in Fig. 2. The material properties of experimental model are obtained by material test, which is shown in Table 2. The natural material properties are used in FEM to make FEM and experimental model the same.

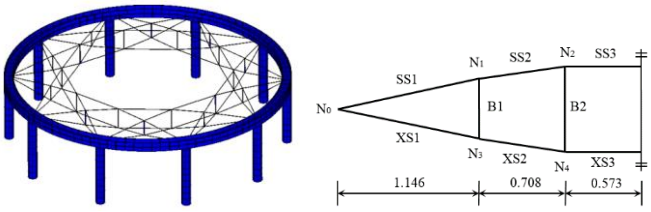

(a) Integral FEM of SCSWIRC (b) Size of planar cable-truss frame

Fig. 1 Integral FEM of SCSWIRC and the size of planar cable-truss frame

Table 1
Feasible pre-stress of FEM

Element number	Cable						Strut	
	SS1	SS2	SS3	XS1	XS2	XS3	B1	B2
Cable length/m	1.157	0.7104	1.146	1.163	0.7106	1.146	0.354	0.463
Non-stress cable length/m	1.153	0.7090	1.142	1.161	0.7094	1.144	-	-
Internal force/kN	3.618	3.573	3.558	2.730	2.712	2.704	-0.349	-0.352

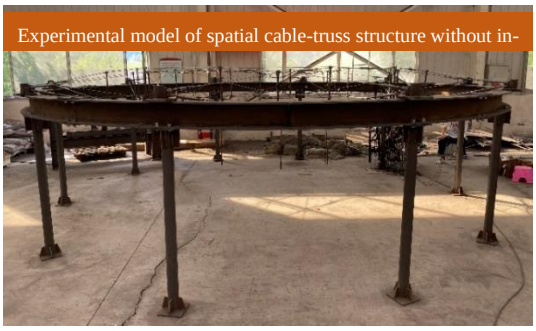

Fig. 2 Integral experimental model of spatial cable-truss structure without inner ring cables

Table 2
Material properties of cable and strut

Element Type	Size	Area/mm^2	Elastic modulus/MPa	Broken force/kN
Cable	Φ6	21.487	$1.21*10^5$	36.00
Strut	P20*3	141.300	$2.05*10^5$	52.02

2.2. Design of Grid-jumped layout schemes

The B1~B10 refers to the number of struts located at the outer ring of experimental model, which is shown in Fig. 3. As the struts located at the inner ring decides the structural outer shape, the rise-span ratio of upper and lower chord cables and drainage slope, the vector height of SCSWIRC is not changed. Namely, the struts located at the inner ring are not removed, so the planar layout diagram of SCSWIRC shown in Fig. 3. Meanwhile, as the span of experimental model is small, three grid-jumped layout schemes are proposed according to the different layout types of struts located at the outer ring. Namely, grid-jumped layout scheme 1 (or Scheme 1) refers to only removing a strut; grid-jumped layout scheme 2 (or Scheme 2) refers to removing struts after every other strut; grid-jumped layout scheme 3 (or Scheme 3) refers to remove all outer ring struts.
Scheme 1: remove B1
Scheme 2: remove B1, B3, B5, B7, B9
Scheme 3: remove B1~B10

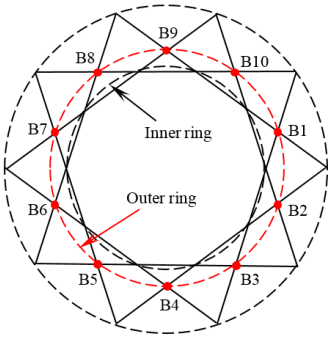

Fig. 3 Planar arrangement diagram of SCSWIRC

In order to easily remove struts located at the outer ring, the particular cable-strut joint is designed and it is shown in Fig. 4a, which is connected by bolts between cables and struts. The cable-strut joints of struts located at the inner ring are shown in Fig. 4b, which is connected by welding between cables and struts.

(a) Joint located at outer ring

(b) Joint located at inner ring

Fig. 4 Cable-strut joint

2.3. Comparative analysis of three grid-jumped layout schemes and original scheme

After construction forming, the feasible pre-stress is near the design pre-stress by repeatedly adjusting the threaded sleeves in two terminals of cables. Meanwhile, when the struts are removed for grid-jumped layout schemes, the lost cable forces are compensated by repeatedly adjusting the threaded sleeves in two terminals of cables.

The feasible pre-stresses of four schemes (original scheme and three grid-jumping layout schemes) in initial states are shown in Table 3 when structural self-weight is considered. The theory values of feasible pre-stresses of four schemes are solved by Ref. [18]. The internal force cloud diagrams of four schemes are shown in Fig. 5.

Table 3
Feasible pre-stresses of four schemes in initial states Unit: kN

Element number	Original scheme			Scheme 1			Scheme 2			Scheme 3		
	E-value	S-value	Error /%	E-value	S-value	Error /%	E-value	S-value	Error /%	E-value	S-value	Error /%
SS1	3.49	3.62	3.56	3.46	3.63	4.89	3.48	3.63	4.31	3.54	3.60	1.77
SS2	3.45	3.57	3.50	3.43	3.62	6.35	3.45	3.62	4.93	3.48	3.59	3.20
SS3	3.41	3.56	4.51	3.43	3.61	5.28	3.50	3.61	2.92	3.45	3.57	3.61
XS1	2.62	2.73	4.02	2.68	2.81	4.70	2.85	2.89	1.18	2.88	2.99	3.70
XS2	2.57	2.71	5.55	2.69	2.81	4.28	2.79	2.81	0.74	2.90	2.99	3.03
XS3	2.68	2.70	0.72	2.66	2.76	4.04	2.72	2.77	2.00	2.88	2.96	2.83
B1	-0.34	-0.35	2.94	-0.44	-0.46	4.50	-0.64	-0.67	4.70	—	—	—
B2	-0.34	-0.35	3.71	-0.46	-0.48	4.37	-0.62	-0.64	3.24	-0.80	-0.81	1.25

Note: E-value stands for experimental value; S-value stands for simulation value.

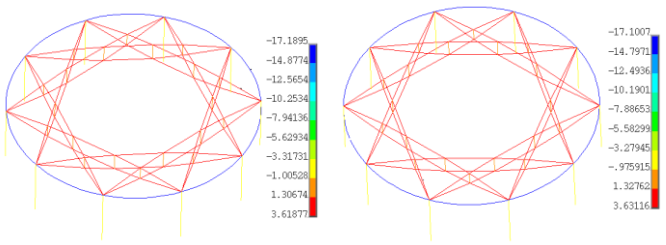

(a) Original scheme (b) Grid-jumped layout scheme 1

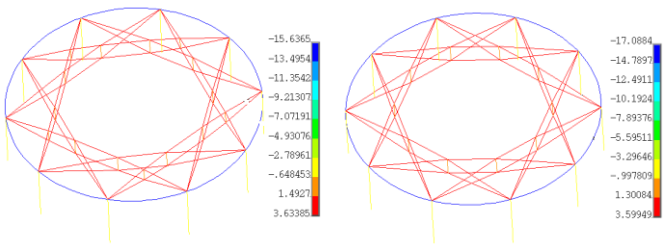

(c) Grid-jumped layout scheme 2 (d) Grid-jumped layout Scheme 3

Fig. 5 Internal force cloud diagram of four schemes

It can be seen from Table 3 that the errors between experimental values and theory values are within 6%, which is acceptable. It can be further concluded

that the grid-jumped layout has a tremendous influence on the nodal displacement and the internal forces of struts, and the grid-jumped layout has negligible influence on the internal forces of cables. Meanwhile, the mechanical property of three grid-jumped layout schemes has not changed compared with original scheme.

The total weight and the number of struts of four schemes are statistically analyzed, and the results are shown in Table 4.

Table 4
Comparison results of the total weight and the number of struts of four schemes

Type	Original scheme	Scheme 1	Scheme 2	Scheme 3
Total weight/kg	25.55	25.15	23.58	21.62
The number of removing struts	0	1	5	10
The amount of saving steel/kg	—	0.39	1.57	1.96
Percent/%	—	1.54	6.24	8.33

It can be seen from Table 4 that the total weight of scheme 3 is the smallest among four schemes. Namely, scheme 3 most saves steel consumption. Meanwhile, scheme 3 has removed 10 struts, so it is the most concise structural type. Scheme 3 is the simplest structural model and it most save structural self-weight.

3. The experimental study of static property

3.1. Static experimental scheme

Based on the experimental model and SHELL154 element, the virtual membrane is built on the grids formed by the upper chord cables of cable-truss frames. The virtual membrane transfers the loads and does not participate in the calculation. Then the membrane loads are chosen as 0.6 kN/m2 according to Ref. [3]. The z-direction constraints are applied to all lower nodes of SCSWIRC, and the constraint reaction forces obtained by finite element analysis are the vertical equivalent nodal loads. The different types of equivalent nodal loads are obtained when the structural self-weight is considered. The equivalent nodal loads are F_{N_1}=-0.429 kN and F_{N_2}=-0.361 kN (the minus sign stands for the vertical direction). The total load is F=10*[F_{N_1}, F_{N_2}]. The N_1 and N_2 are shown in Fig. 1b.

Iron blocks are used to replace the equivalent loads to complete the hierarchical loads in static experiment. The loading process are divided into five steps, including 0.8F, 0.9F, 1.0F, 1.1F, 1.2F. The loading devices are made of PVC membrane, so the self-weight of loading devices is not considered because PVC is very light. The full-span loading and half-span loading experimental models are shown in Fig. 6.

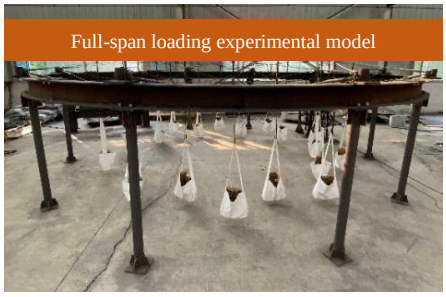

(a) Full-span loading experimental model

(b) Half-span loading experimental model

Fig. 6 Full-span and half-span loading experimental model

As the experimental model comprises 10 planar cable-truss frames, two of 10 planar cable-truss frames are chosen as the monitored objective. The chosen planar cable-truss frames are symmetrically distributed. The monitoring points of internal forces and nodal displacements are shown in Fig. 7a. The strain gauges monitor the change of the internal forces of cables and struts attached to the pre-designed threaded sleeves shown in Fig. 7a. The strain gauges are connected to the static collection instrument JM3813 through collection lines, as shown in Fig. 7b. Static collection instrument JM3813 collects the signals and transmits signals to a computer. Then the signals are converted into strain by computer, and the internal forces of cables and struts can be obtained by further calculations. Level gauge and steel ruler are used to monitor nodal displacements of cable-truss frame at critical positions, shown in Fig. 7c.

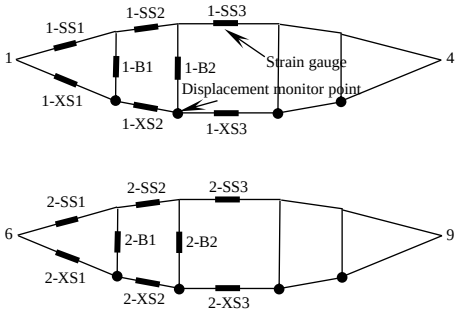

(a) The monitoring points of internal forces and displacements

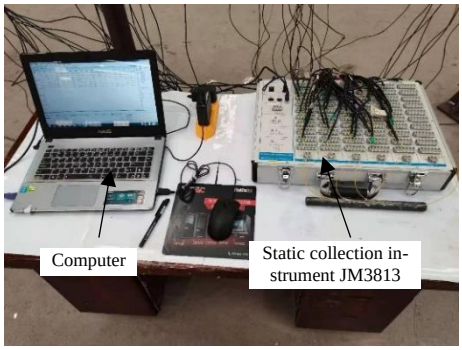

(b) Static collection instrument

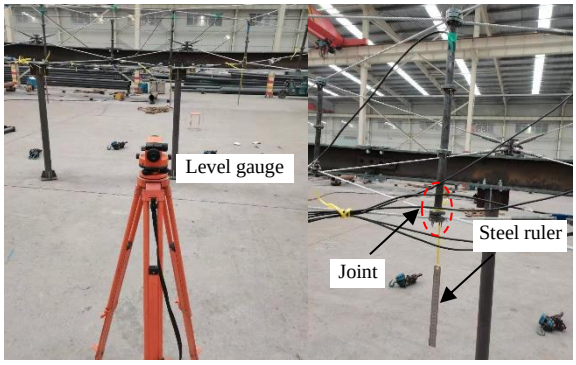

(c) Level gauge and steel ruler

Fig. 7 Static collection instrument JM3813, level gauge and steel ruler

3.2. The static property under the actions of full-span loads

The experimental model is loaded with full-span loads shown in Fig. 6a, and the internal forces and nodal displacements are monitored according to the measuring points in Fig. 7a. The half planar cable-truss frame is taken as a research objective due to the symmetry of structure and loads. The change laws of internal forces and nodal displacements of experimental model and FEM are shown in Fig. 8~Fig. 9 under the actions of full-span loads. The internal forces and nodal displacements of experimental model and FEM are shown in Fig. 10~Fig. 11 under the actions of full-span load 1.0F.

It can be seen from Fig. 8~ Fig. 11 that experimental values agree with simulation values, and the errors are within 10%. Meanwhile, the change laws of experimental values and simulation values are similar. Namely, under full-span loads, the internal forces of upper chord cables and struts gradually decrease with external loads. The internal forces of lower chord cables gradually increase with external loads. So, upper chord cables can loosen when external loads are enormous. It can be known from the comparison results of four schemes that the order of internal forces of all components is scheme 3＞scheme 2＞scheme 1＞original scheme. Under the action of full-span load 1.0F,

the internal forces of upper chord cables have been increased from 2.49 kN in

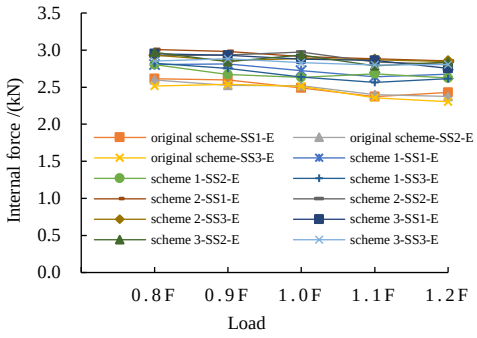

(a) Upper chord cables

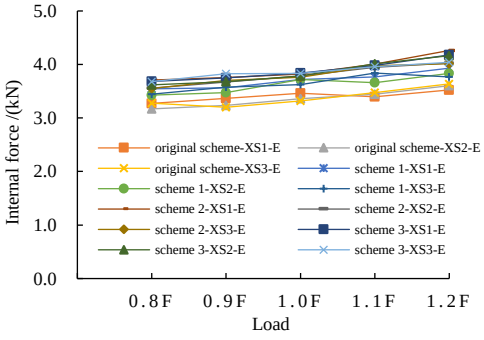

(b) Lower chord cables

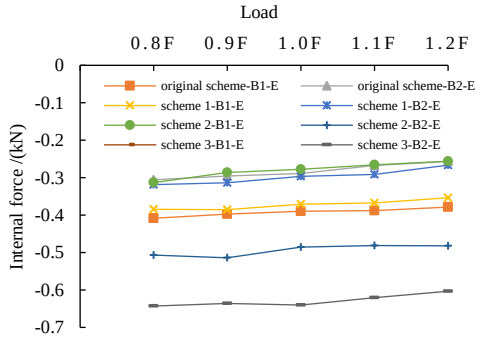

(c) Struts

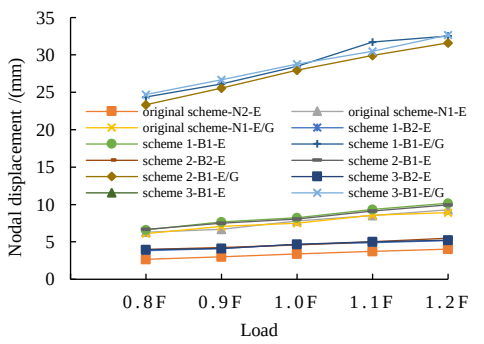

(d) Nodal displacements

Fig. 8 Internal forces and nodal displacements under the actions of full-span loads for experimental model

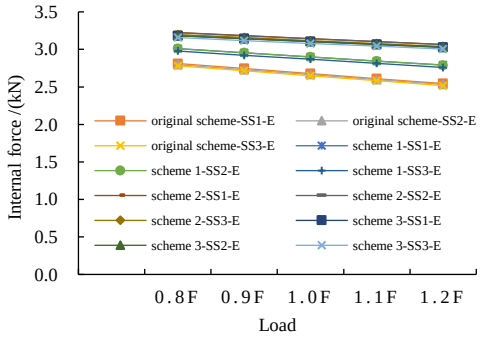

(a) Upper chord cables

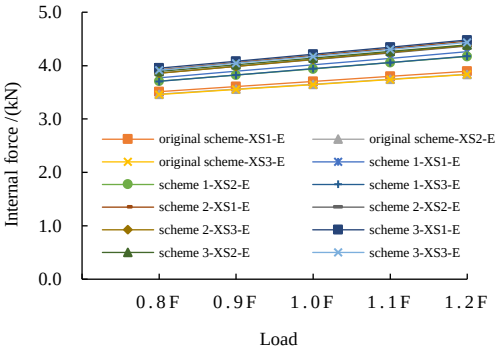

(b) Lower chord cables

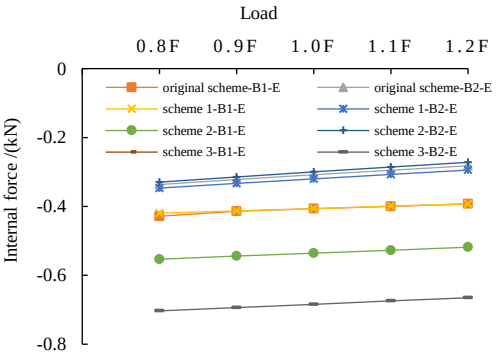

(c) Struts

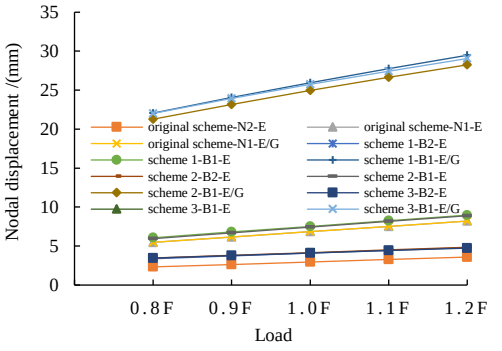

(d) Nodal displacements

Fig. 9 Internal forces and nodal displacements under the actions of full-span loads for FEM

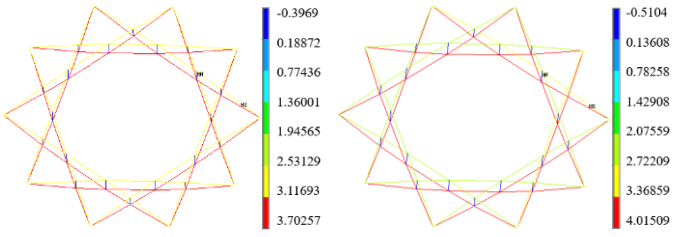

(a) Original scheme (b) Scheme 1

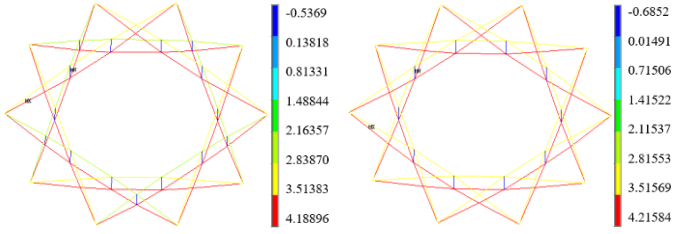

(c) Scheme 2 (d) Scheme 3

Fig. 10 Internal forces of four schemes under the actions of full-span load 1.0F Unit: kN

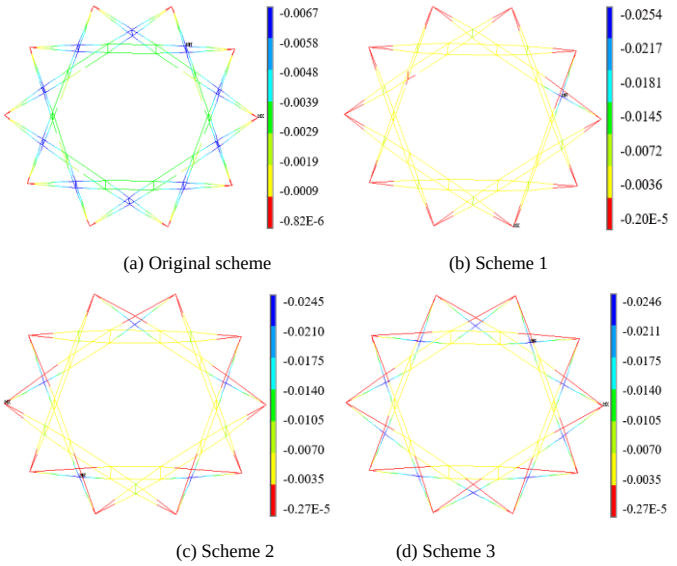

(a) Original scheme (b) Scheme 1

(c) Scheme 2 (d) Scheme 3

Fig. 11 Nodal displacements of four schemes under the actions of full-span load 1.0F
Unit: m

original scheme to 3.11 kN in scheme 3, and it increases by 24.91%; The internal forces of lower chord cables have been increased from 3.46 kN in original scheme to 3.84 kN in scheme 3, and it increases of 10.98%; The internal forces of struts have been increased from -0.39 kN in original scheme to -0.65 kN in scheme 3, and it increases of 66.67%. It can be known that the changes of internal forces of cables are relatively small, and the changes of internal forces of struts are significant after grid-jumped layout.

The order of all nodal displacements is similar to that of internal forces of all components. The maximum nodal displacement of four schemes meets tolerable displacement [δ]=30 mm in Technical Specification of Cable Structures [19], and the nodal displacements of schemes 1~3 are the same. It can be seen from Fig. 8d and Fig. 9d that the nodal displacements at inner ring are smaller than those of the nodal displacements at the outer ring. Meanwhile, the nodal displacements at grid-jumped layout are significantly larger than the nodal displacements at non-grid-jumped layout, which shows grid-jumped layout weakens the local stiffness of SCSWIRC. So, the nodes at grid-jumped layout are more sensitive to external loads, and the designer should pay more attention to internal forces and nodal displacements at grid-jumped layout not to excess the requirements of Code.

3.3. The static property under the actions of half-span loads

The change laws of internal forces and nodal displacements for experimental model and FEM are shown in Fig. 12~Fig. 13 under the actions of half-span loads. The internal forces and nodal displacements of four schemes are shown in Fig. 14~ Fig. 15 under the actions of half-span load 1.0F.

It can be known from Fig. 12~Fig. 15 that experimental values agree with simulation values and experimental values are slightly larger than simulation values. With the increase of the half-span loads, the internal forces of upper chord cables and struts gradually decrease, and the internal forces of lower chord cables gradually increase in the loading part. However, the internal forces of components have no noticeable change in the non-loading part. The change laws of nodal displacements agree with those of internal forces. The maximum internal forces and nodal displacements are scheme 3＞scheme 2＞scheme 1＞original scheme. For the loading part, the internal forces of upper chord cables have been increased from 2.38 kN in original scheme to 3.02 kN in scheme 3, and it increases by 26.89%; The internal forces of lower chord cables have been increased from 3.58 kN in original scheme to 3.92 kN in scheme 3, and it increases of 9.5%; The pressure forces of struts have been increased from 0.35 kN in original scheme to 0.46 kN in scheme 3, and it increases of 82.86%. For the non-loading part, the internal forces of upper chord cables have been increased from 3.23 kN in original scheme to 3.3 kN in scheme 3, and it increases by 1.54%; The internal forces of lower chord cables have been increased from 2.52 kN in original scheme to 2.94 kN in scheme 3 it increases of 16.67%; The pressure forces of struts have been increased from 0.42 kN in original scheme to 0.76 kN in scheme 3. From the comparison results of mechanical property in the non-loading and loading parts, it can be concluded that with the increase of the number of removed struts, the internal forces of struts significantly change and the internal forces of cables change slightly. So, the bearing capacity and stability of struts should be rechecked after grid-jumped layout.

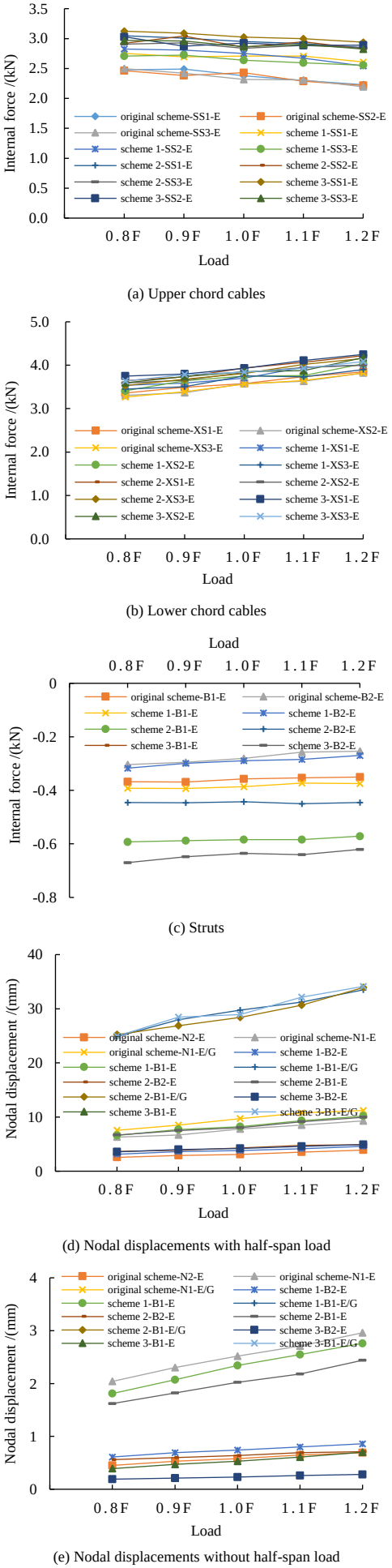

(a) Upper chord cables

(b) Lower chord cables

(c) Struts

(d) Nodal displacements with half-span load

(e) Nodal displacements without half-span load

Fig. 12 Internal forces and nodal displacements under the actions of half-span loads for experimental model

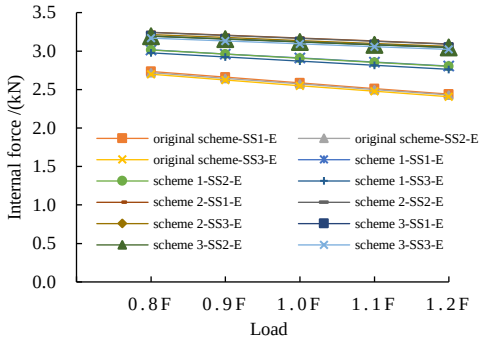

(a) Upper chord cables

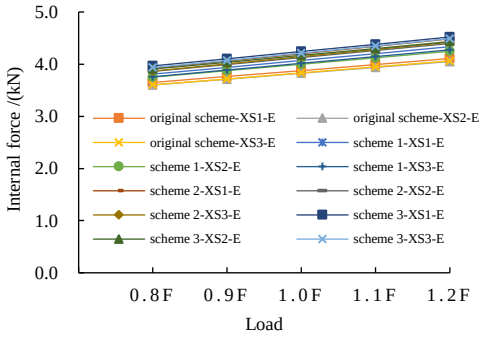

(b) Lower chord cables

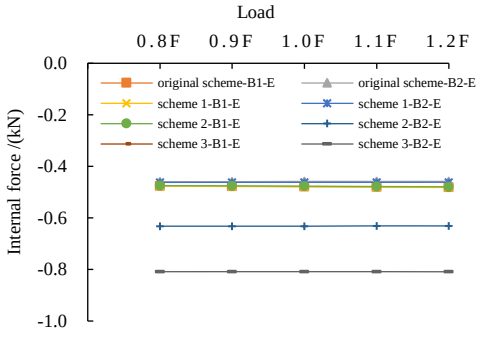

(c) Struts

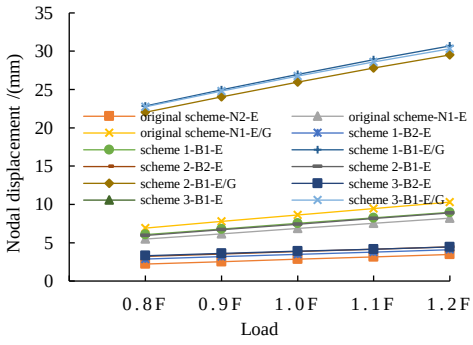

(d) Nodal displacements with half-span load

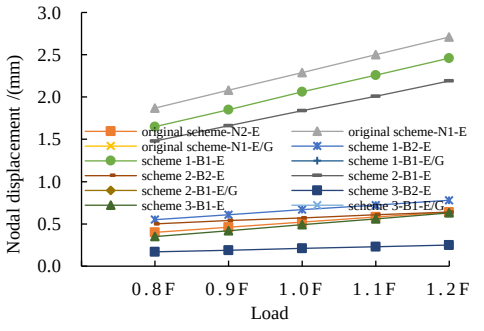

(e) Nodal displacements without half-span load

Fig. 13 Internal forces and nodal displacements under the actions of half-span loads for FEM

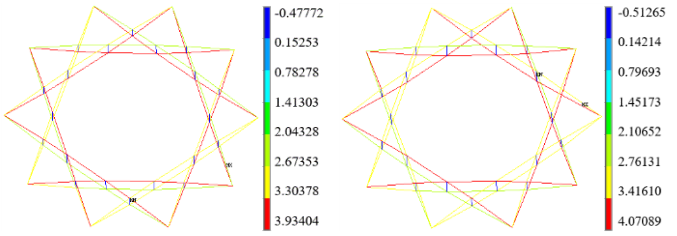

(a) Original scheme (b) Scheme 1

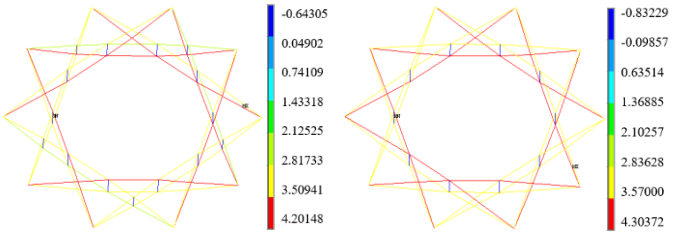

(c) Scheme 2 (d) Scheme 3

Fig. 14 Internal forces of four schemes under the actions of half-span load 1.0F Unit: kN

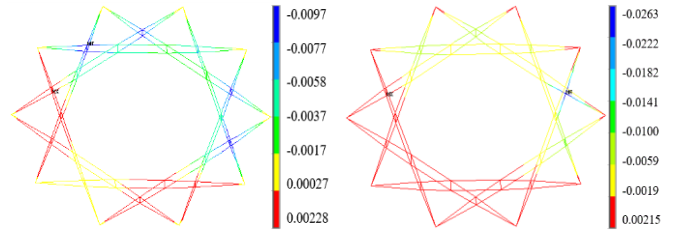

(a) Original scheme (b) Scheme 1

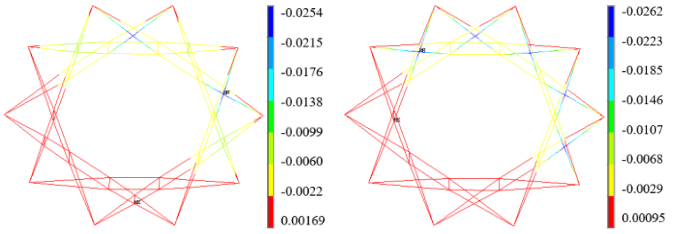

(c) Scheme 2 (d) Scheme 3

Fig. 15 Nodal displacements of four schemes under the actions of half-span load 1.0F Unit: m

3.4. discussions

From the analysis results under the actions of full-span loads and half-span loads, it can be concluded that the optimal grid-jumped layout scheme is scheme 3. Scheme 3 reduces structural self-weight and simplifies structural system. Namely, scheme 3 saves project costs and decreases the difficulty of construction forming.

Form Fig. 8 ~Fig. 9, the errors of internal forces are in the range of 6%~8.91% and the errors of nodal displacements are in the range of 8%~10.27% under the actions of full-span loads. Form Fig. 12 ~Fig. 13, the errors of internal forces are in the range of 8%~10.13% and the errors of nodal displacements are in the range of 9%~11.53% under the actions of half-span loads. From the errors between experimental values and simulation values, the reasons of producing errors mainly include that (1) Measuring devices make errors; (2) Strain gauges make errors; (3) The stiffness of two ends of cables make errors; (4) The manufacturing accuracy of lengths of cables and struts makes errors.

4. The experimental study of dynamic property

4.1. The purpose, theory and scheme of dynamic experiment

4.1.1. The purpose of dynamic experiment

Dynamic experiments can further know the effects of grid-jumped layout on the dynamic property of SCSWIRC. At the same time, the natural frequency, damping ratio and vibration mode of SCSWIRC can be obtained by dynamic experiments. Natural frequency, damping ratio and vibration mode are the most

critical three parameters that reflect the capacity of bearing dynamic loads and evaluate the structural dynamic property. The three parameters are also the basis of wind spectrum analysis and seismic response spectrum analysis. So, it is necessary to further study the effects of grid-jumped layout on the dynamic property of SCSWIRC.

4.1.2. The theory of dynamic experiment

SCSWIRC is a kind of tensile structure, which is a very flexible structure, so the grid-jumped layout of struts will reduce structural stiffness in the experiment. As the structural self-weight is light, the hammer is used to apply inspiration to acceleration sensors in experimental model. The dynamic collection instrument JM3841 is sued to collect the signals of acceleration sensor arranged at some nodes. Then put the obtained signals into the dynamic collection instrument JM3841, and the corresponding acceleration time history curves can be obtained by JM3841 Software. The corresponding frequency spectrum curves can be obtained based on the obtained signals through frequency spectrum analysis. The maximum values of frequency spectrum curves are the natural frequencies of structures. The structural damping ratio can be calculated according to the vibration attenuation curve of measuring points based on the viscous damping theory.

The calculation equation of damping ratio is as follows:

$$\ln \frac{y_n}{y_{n+1}} = \xi\omega \frac{2\pi}{\omega'} \tag{2}$$

In Eq. (2), y_n and y_{n+1} illustrate the amplitude significance of one week apart; ξ is the damping ratio; ω and ω' stand for the undamped and damped vibration frequency, respectively.

It is assumed that δ is the logarithmic attenuation rate of vibration amplitude, and δ is as follows:

$$\delta = \ln \frac{y_n}{y_{n+1}} \tag{3}$$

So, Eq. (2) can be written as Eq. (4):

$$\zeta = \frac{\delta}{2\pi} \frac{1}{\sqrt{1+(\delta/2\pi)^2}} \tag{4}$$

When $\xi < 0.2$, the Eq. (4) can be written as Eq. (5):

$$\zeta = \frac{\delta}{2\pi} \tag{5}$$

In order to reduce the effects of external excitation on the dynamic experiment, each excitation point is subjected to 10 times excitation, and the average values of 3 times experimental results are used as the final experimental values.

4.1.3. Experimental scheme

The dynamic collection instrument JM3841 is used in the experiment, shown in Fig. 16a. The IEPE acceleration sensors are used in the dynamic experiment, shown in Fig. 16b. The acceleration sensor has the advantages of lightness, little volume, a wide frequency response range and high stability, which is suitable for the dynamic experiment. The layout diagram of acceleration sensors is shown in Fig. 16c. The acceleration time-history curve of measuring point A-2 is shown in Fig. 16d. In the experiment, the external excitation is produced by hammering and hammering the excitation points every 30 s for 5 min at the same time, and then two sets of data are collected.

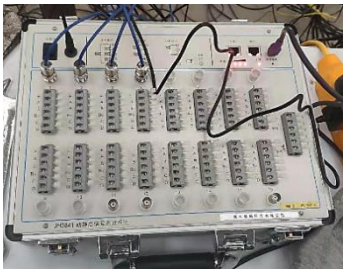

(a) Dynamic collection instrument JM3841

(b) Acceleration sensor

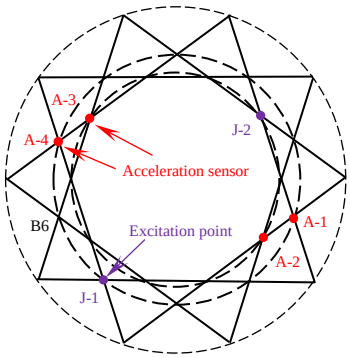

(c) Layout diagram of acceleration sensors

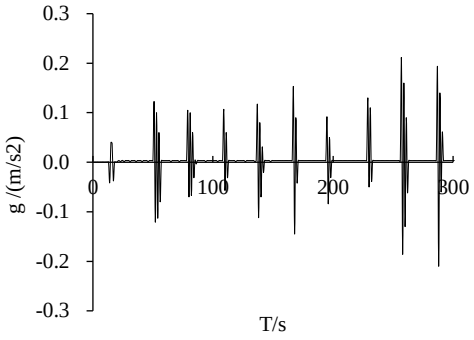

(d) Time-history curve of acceleration sensor

Fig. 16 Correlation diagrams of experimental model

As the torsional rigidity of experimental model is relatively large, the first few modes are all vertical. Meanwhile, there is the deformation coupling phenomenon in each mode of experimental model. Regarding structural symmetry, adjacent frequencies may have slight differences and it is difficult to identify all frequencies. Meanwhile, there are some errors between the site environment and dynamic collection instrument in the process of collecting signals, so the partial frequencies are obtained in the dynamic experiment.

4.2. The dynamic property under the actions of non-loads

The natural frequencies and damping ratio of four schemes under the actions of no external loads are shown in Table 5 and Table 6.

Table 5
Natural frequencies of four schemes in initial state

Order of frequency	Original scheme /HZ		Scheme 1 /HZ		Scheme 2 /HZ		Scheme 3 /HZ	
	Trial Value	Theory Value	Trial Value	Theory Value	Trial Value	Theory Value	Trial Value	Theory Value
1	6.409	6.742	4.571	5.065	6.531	6.768	4.700	5.053
3	6.922	7.296	—	6.945	—	7.023	—	5.064
5	—	8.573	7.089	7.790	7.584	7.214	—	5.097
7	8.734	9.087	—	8.806	8.553	8.703	—	5.159

Table 6
Damping ratio of experimental model in initial state

Order of frequency	Original scheme	Scheme 1	Scheme 2	Scheme 3
1	0.0099	0.0090	0.0153	0.0198
3	0.0174	—	—	—
5	—	0.0159	0.0065	—
7	0.0190	—	0.0075	—

From Table 5, the experimental values of natural frequency agree with the simulation values. The maximum error is 7.6%, and most errors are within 6%~7%, which shows that simulation values agree with experimental values. As the experimental model is symmetric, there are many similar frequencies, so the partial frequencies are identified in the experimental model. It can be seen from Table 6 that the damping ratios of structure are little in initial state, which is within 0.02.

4.3. The dynamic property under the actions of full-span loads

Generally speaking, the structural natural frequency is an inherent feature

not correlated with external loads. However, external loads can be equivalent to extra mass in dynamic analysis so that external loads will affect the natural feature of structure.

In order to study the natural vibration of different grid-jumped layout schemes with the change of extra mass (or external loads), the natural frequency and damping ratio of experimental model are studied under the actions of full-span loads and half-span loads. The external loads are replaced with iron blocks shown in Fig. 6, which is applied on the lower nodes of experimental model. The extra mass is divided into five steps, similar to Section 3. The experimental and simulation values of natural frequency for four schemes are shown in Fig. 17 under the actions of full-span loads. As the 1st, 3rd, 5th, 7th order frequencies are equal to the 2nd, 4th, 6th, 8th order frequencies, the 1st, 3rd, 5th, 7th order frequencies are given in Fig. 17. The vibration modes of four schemes under the actions of full-span load 1.0F are shown in Fig. 18.

It can be seen from Fig. 17 and Fig. 18 that the experimental values and simulation values of natural frequencies are similar under the actions of full-span loads. The errors between experimental values and simulation values of natural frequencies are within 11.75%, and the errors mainly focus on the range of 6%~8%. The order of natural frequencies of four schemes is original scheme ＞scheme 1＞scheme 2＞scheme 3, and the natural frequencies of four schemes are near at the same time. The natural frequencies of four schemes gradually increase with the increase of external loads. The main reason is that the structural mass becomes more extensive, and the natural frequencies of four schemes become small when the external loads are converted into structural mass. The grid-jumped layout has changed structural high order frequencies.

Meanwhile, grid-jumped layout has changed the local stiffness of structure and further changed its vibration modes. However, the first vibration mode of four schemes is the upper and lower vibration accompanied by the local torsion of planar cable-truss frames. It can be known from Ref. [13] that there is no harm to the structure when the first vibration mode is the local torsion of planar cable-truss frames. So, the dynamic property of the four schemes is rather good.

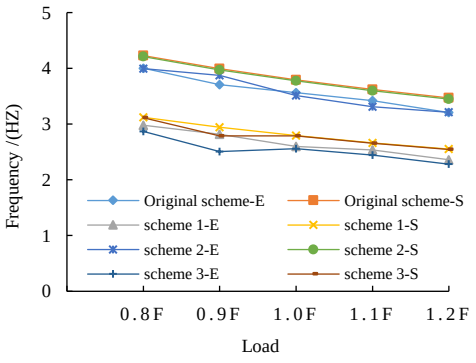

(a) First order frequency

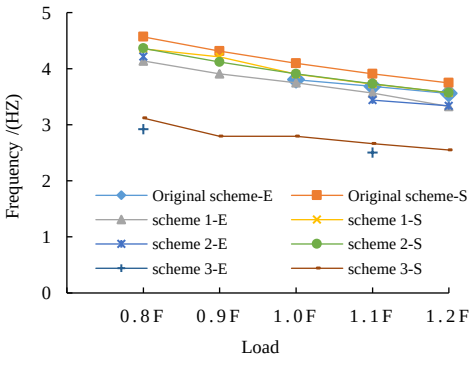

(b) Third order frequency

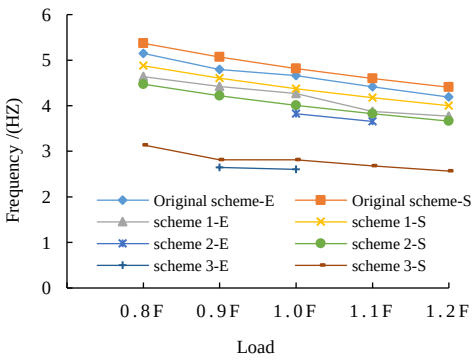

(c) Fifth order frequency

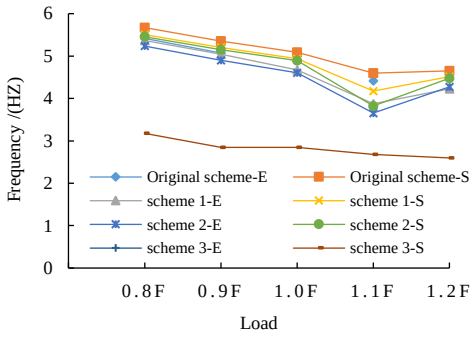

(d) Seventh order frequency

Fig. 17 The comparison results of natural frequencies of four schemes under the actions of full-span loads

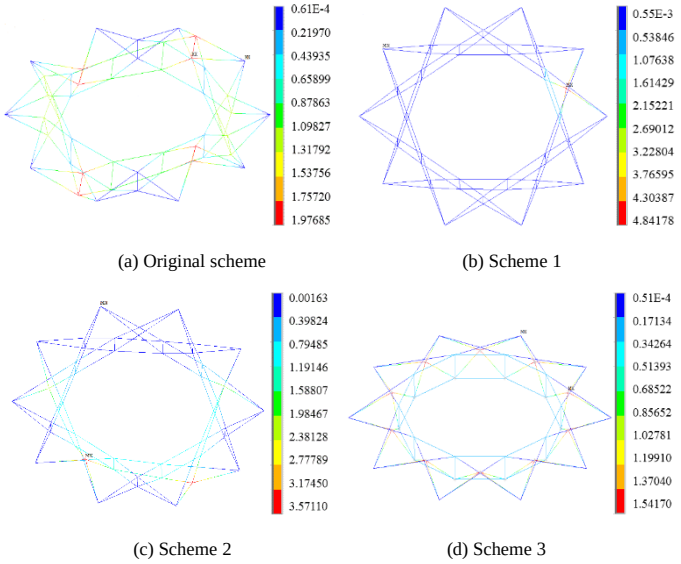

(a) Original scheme (b) Scheme 1

(c) Scheme 2 (d) Scheme 3

Fig. 18 First vibration modes of four schemes under the actions of full-span load 1.0F

4.4. The dynamic property under the actions of half-span loads

The experimental and simulation values of natural frequency for four schemes under the actions of half-span loads are shown in Fig. 19. The first vibration modes of four schemes under the actions of half-span load 1.0F are shown in Fig. 20. The experimental values of damping ratios of four schemes under the actions of full-span and half-span loads are shown in Table 7.

It can be seen from Fig. 19 and Fig. 20 that the most error between experimental values and simulation values of natural frequencies is 10.06% for four schemes, and the errors mainly focus on the range of 5%~7%. Experimental values agree with simulation values, which verify the experiment is correct, and experimental results can reflect on the fundamental property of structure. The grid-jumped layout changes the structural high order frequency.

Meanwhile, grid-jumped layout also changes the local stiffness of structure and further changes the structural vibration modes. However, the first vibration

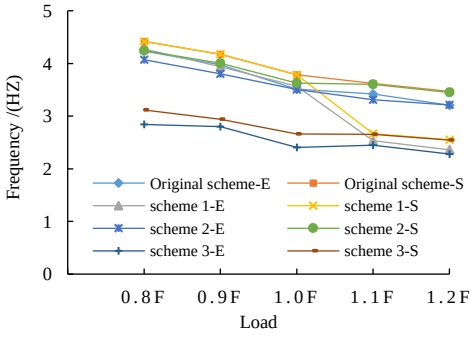

(a) First order frequency

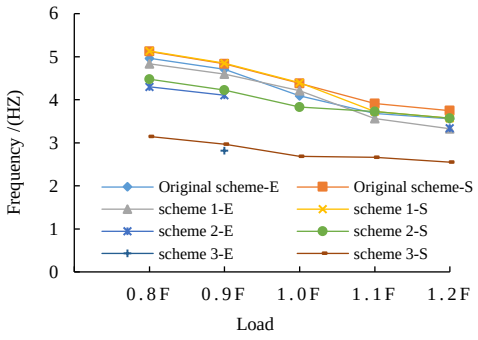

(b) Third order frequency

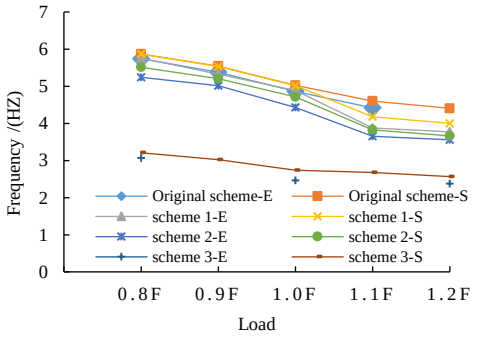

(c) Fifth order frequency

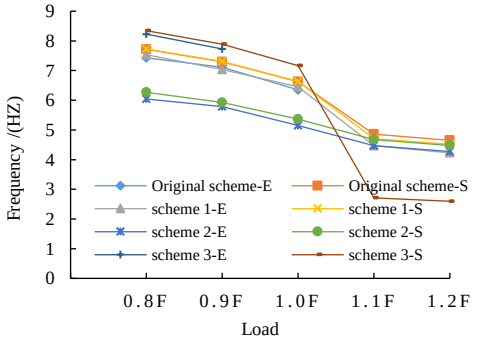

(d) Seventh order frequency

Fig. 19 The comparison results of natural frequencies of four schemes under the actions of half-span loads

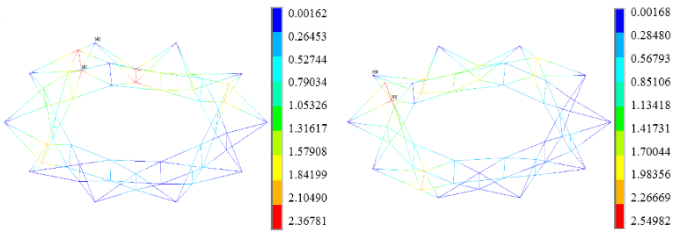

(a) Original scheme (b) Scheme 1

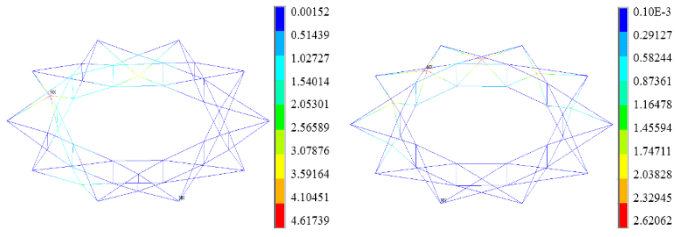

(c) Scheme 2 (d) Scheme 3

Fig. 20 First vibration modes of four schemes under the actions of half-span load 1.0F

mode of four schemes is upper and lower vibration accompanied by the local torsion of planar cable-truss frames. It can be known from Ref. [13] that there is no harm to structure when the first vibration mode is the local torsion of planar cable-truss frames. So, the dynamic property of the four schemes is rather good.

4.5. Damping ratio of experimental model

From the measured data of damping ratio, the damping ratios corresponding to all different natural frequencies are in the range of 0.005~0.02. The damping ratios of four schemes do not change with the order of frequency. Generally speaking, the external loads affect structural damping ratios. However, it is not found that the damping ratios of four schemes changes with the change of external loads during the experiment. The experimental values of damping ratios of four schemes are shown in Table 7 under the actions of full-span loads and half-span loads.

5. Further discussions

Although the span of experimental model is 6 m, the relative conclusions can explain the actions and effects of grid-jumped layout on SCSWIRC. In order to further explain the actions and meanings of grid-jumped layout, the SCSWIRC with the span of 100 m is given, shown in Fig. 21a.

The struts at virtual inner ring are not removed because the struts at virtual inner ring decide drainage slope, outer shape and the rise-span ratio of upper and lower chord cables. According to the SCSWIRC in Fig. 21a and the positions of grid-jumped layout, the three grid-jumped layout schemes can be proposed. The three grid-jumped layout schemes include grid-jumped layout scheme 1 (scheme 1), grid-jumped layout scheme 2 (scheme 2), and grid-jumped layout 3 (scheme 3). In Fig. 21b, scheme 1 refers to removing the struts at inner ring 1; scheme 2 refers to removing the struts at inner ring 2; scheme 3 refers to removing the struts at inner ring 3.

The optimal grid-jumped layout schemes can be obtained by using the same analysis method as experimental model in Section 2. The optimal grid-jumped layout scheme is scheme 1. The optimal scheme 1 simplifies structural system and reduces forming construction difficulty and structural self-weight, and saves costs.

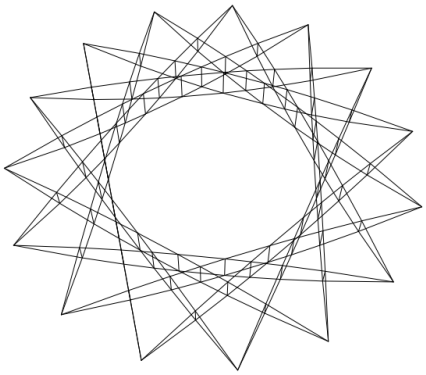

(a) SCSWIRC with a span of 100 m

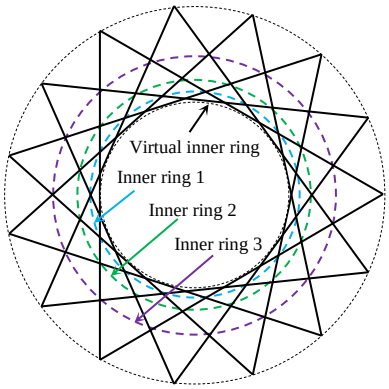

(b) Planar diagram of grid-jumped layout

Fig. 21 Perspective diagram and planar diagram of grid-jumped layout of SCSWIRC

When the span of SCSWIRC does not exceed 400 m, the strut can be the form of a circular steel pipe. When the span of SCSWIRC is larger than 400 m, the length of struts will be too long. In order to reduce the crossed-sectional areas of struts and enhance the stiffness and stability of struts, the form of struts can be the form of an open-web fusiform truss shown in Fig. 22a. The open-web fusiform truss can be divided into different lattice column forms, shown in Fig. 22b. The different lattice columns can be connected by bolt and weld.

Table 7
Experimental values of damping ratios of four schemes under the actions of full-span and half-span loads

Order of frequency	Damping ratios under the actions of full-span loads				Damping ratios under the actions of half-span loads			
	Original scheme	Scheme 1	Scheme 2	Scheme 3	Original scheme	Scheme 1	Scheme 2	Scheme 3
1st	0.01917	0.01646	0.0134	0.00621	0.01831	0.01789	0.00797	0.01843
3rd	0.01764	0.01256	—	—	0.01261	0.00512	—	—
5th	0.01404	0.01355	0.00982	0.0087	0.01303	0.01846	0.01935	0.01278
7th	—	0.01732	0.01732	—	0.01109	0.00953	0.01653	—

The design recommendations for SCSWIRC based on the above discussions include: (1) Cable-strut joints are essential for the mechanical property of structure, so cable-strut joints can make the cable forces of all kinds of cables pass smoothly. (2) The grid-jumped layout can simplify structure when original scheme is already decided, which can reduce self-weight and save project costs. (3) The structural rise should meet drainage slope and optimal rise, which is beneficial for the structural mechanical property. (4) The suitable construction method and construction steps should be considered in the design. (5) The influences of wind load on SCSWIRC should be further considered because it belongs to flexible tensile structures.

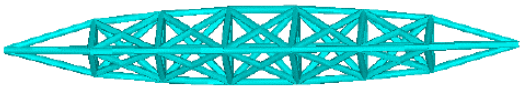

(a) Open-web fusiform truss

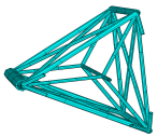

(b) Lattice column

Fig. 22 Relative diagram of open-web fusiform truss

6. Conclusions

Based on the above studies and discussions, some conclusions can be given as follows:

(1) The three grid-jumped layout schemes are proposed according to the exper imental model. The results of static experiment show that the change laws of mechanical property for SCSWIRC are similar. The experimental values are agree with simulation values. The errors mainly focus on the range of 6%~10.27% under the actions of full-span loads, and the errors mainly focus on the range of 8%~11.53% under the actions of half-span loads.

(2) The grid-jumped layout has minor effects on the internal forces of cables. It dramatically affects the nodal displacements and the internal forces of struts at the grid-jumped layout, so the strength and stability of struts should be rechecked after grid-jumped layout.

(3) The results of dynamic experiment show that the errors of natural frequencies primarily focus on the range of 6%~8% and 5%~7% under the actions of full-span and half-span loads, respectively. The grid-jumped layout has changed structural local stiffness and vibration modes, but the first vibration mode of four schemes is upper and lower vibration accompanied by the local torsion of planar cable-truss frames, which is not harmful to SCSWIRC.

(4) The results of static and dynamic experiments show that the grid-jumped layout has not changed the basic mechanical property of SCSWIRC and the optimal grid-jumped layout scheme is scheme 3. The optimal scheme 3 removes the redundant struts, simplifies structural system, reduces structural self-weight, and saves project costs.

Acknowledgements

The authors would like to acknowledge the financial support of the National Natural Science Foundation of China (51778017). Acknowledge graduated students Renqi Ji and Runsheng Zhao for their efforts in experiment. Thank Majid Dezhkam for helping me revising grammar errors in language.

References

[1] Guo Y L. Tian G Y. Cable structure system, design theory and construction control. Beijing: Science Press, 2014.
[2] Guo Y L, Zhang X Q. Influence of temperature changes and cable length errors on tension structures using un-adjustable cable length design. China Civil Engineering Journal, 2017, 50(6): 11-22.
[3] Guo J M, Jiang J Q. An algorithm for calculating the feasible pre-stress of cable-struts structure. Engineering Structure, 2016, 118(1), 228-39.
[4] Chen L M, Hu D, Gao W F, Dong S L, Zhou Y Y, Zhang F B. (2018). Support node construction error analysis of a cable-strut tensile structure based on the reliability. Advances in Structural Engineering, 2008, 21(10), 1553-1516.
[5] Zhang A L, Sun C, Jiang Z Q. Experimental study on the construction shape-forming process and static behavior of a double strut cable dome. Journal of Zhejiang University-Science (Applied Physics and Engineering), 2018, 19(03), 225-239
[6] Ge J Q, Zhang A L, Liu X G, Zhang G J, Ye X B, Wang S, Liu X C. Analysis of tension form-finding and whole loading process simulation of cable dome structure. Journal of building structures, 2012, 33(04):1-11.
[7] Deng H, Zhang M R, Liu H C, Dong S L, Zhang Z H, Chen L Q. Numerical analysis of the pretension deviations of novel Crescent-shaped tensile canopy structural system, Engineering Structures, 2016, 119, 24-33.
[8] Zhang W J, Hu S L, Zhang Y G. A review on progressive collapse of large-span space structure. The 9th National Modern Structure Engineering, Jinan, 2009: 334-338.
[9] Lu J, Li X Y, Xue S D, Liu R J, Majid D. Study on force Mechanism of Cable-truss Frame and jumped layout of Annular Crossed Cable-truss Structure, Advanced Steel Construction, 2021, 17(03), 243~252.
[10] Lu J, Xue S D, Li X Y, Liu R J. Study on membrane roof schemes of annular crossed cable-truss structure. International Journal of Space Structures, 2019, 34(3-4):85-96.
[11] Huang H, Xian Y Q, Xi K L, Liu B Q. Experimental study and numerical analysis on the progressive collapse resistance of SCMS. International Journal of Steel Structures, 2019, 19(01): 301-318.
[12] Zhao R, Wei D M, Sun W B, Xu M. Form-finding method of cable-membrane structures considering cable force-finding form appropriate moment. International Symposium on Innovation and Sustainability of Structures in Civil Engineering, Guangzhou, PEOPLES R CHINA, 2009: 814-818.
[13] Guo Y L, Wang K, Tian G Y, Zhang B H. Research and design of structural form of spoke structure. Journal of Building Structures, 2013, 34(5): 11−19.
[14] Jeon B, Lee J. Cable membrane roof structure with oval opening of stadium for 2002 FIFA world Cup in Busan. In: Proceedings of sixth Asian-Pacific conference on shell and spatial structures, 2000, 2, 1037-42.
[15] Liu R J, Xue S D, Li X Y. Preventing disproportionate displacements in an annular crossed cable-truss structure, International Journal of Space Structures, 2017, 32(1), 3-10.
[16] Liu R J, Li X Y, Xue S D. Experimental and numerical research on Annular Crossed Cable Truss Structure under cable rupture, Earthquake Engineering and Engineering Vibration, 2017, 16(3), 557-569.
[17] Shen S D, Xu C B, Zhao C, W Y. Suspension structure design. Beijing: China Architecture & Building Press, 2006.
[18] Xue S D, Lu Jian, Li X Y, Liu R J. Improved force iteration method based on rational shape design solving self-stress modes of cable-truss tensile structure, Advanced Steel Construction. 2020, 16(2), 170-180.
[19] Technical Specification for Cable Structure, JGJ257-2012. Beijing: China Architecture & Building Press, 2008.